JOURNAL OF GUIDANCE, CONTROL, AND DYNAMICS
Vol. 21, No. 5, September–October 1998

Dynamics, Stability, and Control of Displaced Non-Keplerian Orbits

Colin R. McInnes*
University of Glasgow, Glasgow, Scotland G12 8QQ, United Kingdom

The dynamics, stability, and control of a large family of non-Keplerian orbits are investigated and mission applications are discussed. The orbits are generated by seeking equilibrium solutions to the two-body problem in a rotating frame of reference with an additional thrust-induced acceleration. Viewed from an inertial frame of reference, displaced circular orbits are obtained. Three main families of orbits are presented, and their local stability characteristics are investigated. Although it is found that there are unstable subfamilies of orbits, it is also shown that these orbits are controllable using linear state feedback. Impulse control is also investigated as a means of generating displaced orbits and is compared to continuous thrust control. It is demonstrated that these non-Keplerian orbits can be patched together to provide large additional families of orbits.

Nomenclature

$\boldsymbol{a}$, a	= acceleration, semimajor axis
e, E	= eccentricity, total energy
$\boldsymbol{n}$	= thrust vector orientation
$\boldsymbol{r}$, r	= position, orbit radius
T	= spacecraft thrust, impulse period
U	= augmented potential
z	= out-of-plane displacement
α, $\delta\alpha$	= pitch angle, pitch control
γ	= mode eigenfrequency
η	= vertical perturbation
λ, Λ	= variational equation coefficients, coefficient matrix
μ	= gravitational parameter
ξ	= radial perturbation
ρ	= orbit radius (cylindrical coordinates)
$\boldsymbol{\sigma}$	= generalized displacement
υ	= centripetal potential
ϕ, Φ	= azimuthal angle, gravitational potential
ψ	= azimuthal perturbation
$\boldsymbol{\omega}$, ω	= orbital angular velocity
$\hat{}$	= unit vector

I. Introduction

DISPLACED non-Keplerian orbits generated using low-thrust propulsion have been considered by various authors for applications to spacecraft proximity maneuvering[1] and in situ observations of Saturn's rings.[2] Large families of displaced orbits have also been investigated for solar sail spacecraft.[3–5] One such family of orbits has been recently noted as a particular solution to the two-body problem with radiation pressure in Kustaanheimo–Stiefel (KS) variables.[6]

In this paper, the two-body problem is considered with an additional thrust-induced acceleration, which generates large families of circular non-Keplerian orbits with their center displaced above the central body.[7] The problem is parameterized by the spacecraft orbit period, which generates several families of orbits. The linear stability properties of the orbit families are then investigated and unstable subfamilies of orbits identified. However, it is found that these orbit families are controllable using linear state feedback to the thrust-induced acceleration direction or magnitude. Displaced spiral orbits are also obtained through the addition of an azimuthal component of thrust. Last, additional families of orbits are obtained by patching displaced non-Keplerian orbits to other displaced orbits or Keplerian orbits.

Although it is found that only small displacements are possible for a large central body and low-thrust propulsion, there are potentially useful applications. For example, an orbit displaced 20 km above Saturn's A ring only requires an acceleration of order 0.4 mms^{-2}, corresponding to an accumulated Δv per orbit of 18 ms^{-1}. Such an orbit provides an ideal but safe location for in situ observations in close proximity to the ring system.

II. Displaced Non-Keplerian Orbits

The conditions for circular displaced non-Keplerian orbits will now be investigated by considering the dynamics of a spacecraft of mass m at position $\boldsymbol{r}$ in a rotating frame of reference $R(x, y, z)$. This frame of reference rotates with constant angular velocity $\boldsymbol{\omega} = \omega\hat{\boldsymbol{z}}$ relative to an inertial frame $I(X, Y, Z)$, as shown in Fig. 1. It will be assumed that the spacecraft has active propulsion generating thrust T in direction $\boldsymbol{n}$, where the thrust-induced acceleration is assumed constant in magnitude.

The equation of motion of the spacecraft in the rotating frame R is then given by

$$\ddot{\boldsymbol{r}} + 2\boldsymbol{\omega} \times \dot{\boldsymbol{r}} + \boldsymbol{\omega} \times (\boldsymbol{\omega} \times \boldsymbol{r}) = \boldsymbol{a} - \nabla\Phi \tag{1}$$

where gravitational potential Φ of the central body and the thrust-induced acceleration $\boldsymbol{a}$ are defined as

$$\Phi = -(\mu/r), \qquad \boldsymbol{a} = [T/m]\boldsymbol{n} \tag{2}$$

Equation (1) may be simplified by introducing a new potential υ to represent the centripetal acceleration, viz.,

$$\nabla\upsilon = \boldsymbol{\omega} \times (\boldsymbol{\omega} \times \boldsymbol{r}), \qquad \upsilon = -\tfrac{1}{2}\|\boldsymbol{\omega} \times \boldsymbol{r}\|^2 \tag{3}$$

Defining a new augmented potential function $U = \Phi + \upsilon$, the equation of motion is then given by

$$\ddot{\boldsymbol{r}} + 2\boldsymbol{\omega} \times \dot{\boldsymbol{r}} + \nabla U = \boldsymbol{a} \tag{4}$$

The conditions for equilibrium solutions in the rotating frame of reference will now be obtained by setting $\dot{\boldsymbol{r}}$ and $\ddot{\boldsymbol{r}} = 0$ so that the first two terms in Eq. (4) vanish. Taking the vector product of $\boldsymbol{n}$ with Eq. (4) it is found that

$$\nabla U \times \boldsymbol{n} = 0 \Rightarrow \boldsymbol{n} = \lambda\nabla U \tag{5}$$

where λ is an arbitrary scalar multiplier. Then, using the normalization condition $\|\boldsymbol{n}\| = 1$, λ is identified as $\|\nabla U(\boldsymbol{r})\|^{-1}$. The required thrust vector orientation for an equilibrium solution in the rotating frame is then given by

$$\boldsymbol{n} = \frac{\nabla U}{\|\nabla U\|} \tag{6}$$

Received June 2, 1997; revision received Feb. 25, 1998; accepted for publication March 11, 1998.

*Reader, Department of Aerospace Engineering. E-mail: colinmc@aero.gla.uc.uk.

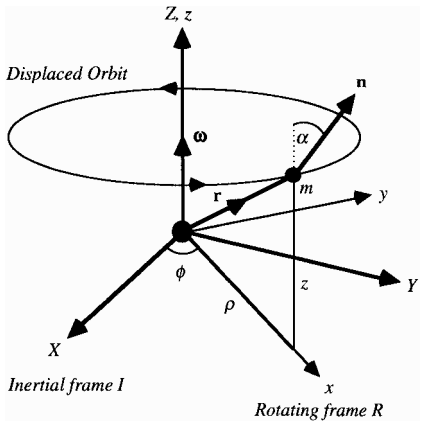

Fig. 1 Displaced non-Keplerian orbit with thrust-induced acceleration.

Because $\boldsymbol{\omega}$ is constant, there can be no transverse component of thrust so that the thrust vector is pitched in the plane spanned by the radius vector and the vertical axis. Therefore, the thrust vector orientation may be defined by a single pitch angle α:

$$\tan\alpha = \frac{\|\hat{z} \times \nabla U\|}{\hat{z} \cdot \nabla U} \tag{7}$$

If we again require an equilibrium solution in the rotating frame so that $\boldsymbol{a} = \nabla U$, it is clear that the magnitude of the thrust-induced acceleration is given simply by

$$a = \|\nabla U\| \tag{8}$$

Therefore, Eqs. (7) and (8) will define the conditions for an equilibrium solution to the equations of motion in the rotating frame of reference. Using a set of cylindrical polar coordinates, as shown in Fig. 1, the potential U may be written as

$$U(\rho, z; \omega) = -\left[\tfrac{1}{2}(\omega\rho)^2 + (\mu/r)\right] \tag{9}$$

Then, the required pitch angle and thrust-induced acceleration are found to be

$$\tan\alpha(\rho, z; \omega) = (\rho/z)\left[1 - (\omega/\omega_*)^2\right], \qquad \omega_*^2 = \mu/r^3 \tag{10a}$$

$$a(\rho, z; \omega) = \left[\rho^2\left(\omega^2 - \omega_*^2\right)^2 + z^2\omega_*^4\right]^{\frac{1}{2}} \tag{10b}$$

With these conditions the spacecraft is stationary in the rotating frame of reference. Therefore, from an inertial frame of reference it appears to execute a circular orbit displaced above the central body. It should be noted that because the vector $\boldsymbol{n}$ is fixed in the rotating frame it sweeps out a cone in the inertial frame of reference.

III. Families of Displaced Orbits

Type I Orbits

It can be seen from Eq. (10b) that the required thrust-induced acceleration has a global minimum when the orbit period is chosen such that $\omega = \omega_*$. Then, the required pitch angle and thrust-induced acceleration are given simply by

$$\tan\alpha = 0 \tag{11a}$$

$$a = \mu z/r^3 \tag{11b}$$

It is clear that the required acceleration a is now a function solely of the orbit radius ρ and displacement z. The functional form of Eq. (11b) is shown as a contour plot in Fig. 2a. The axes are nondimensional with respect to the radius of the central body, whereas the acceleration contours are nondimensional with respect to the gravitational acceleration at unit radius. Thus, the final contour in Fig. 2a, which intersects the z axis at $z = 10$, requires a nondimensional acceleration of 10^{-2}. This corresponds to a single equilibrium point with the thrust-induced acceleration exactly balancing local gravity.

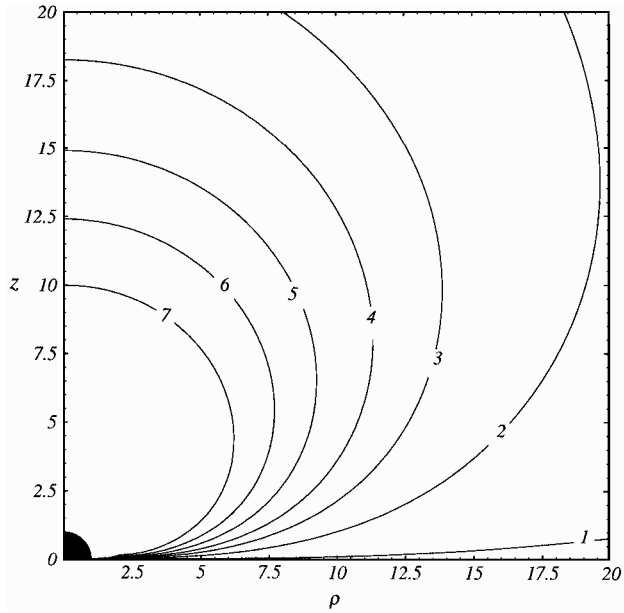

Fig. 2a Nondimensional acceleration contours for type I orbits: contour 1, 1×10^{-4}; contour 2, 1×10^{-3}; contour 3, 2×10^{-3}; contour 4, 3×10^{-3}; contour 5, 4.5×10^{-3}; contour 6, 6.5×10^{-3}; and contour 7, 1×10^{-2}.

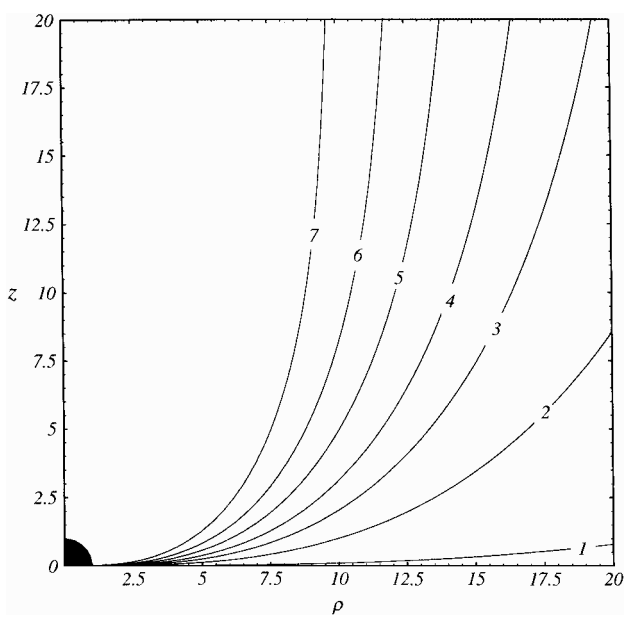

Fig. 2b Nondimensional acceleration contours for type II orbits: contour 1, 1×10^{-4}; contour 2, 1×10^{-3}; contour 3, 2×10^{-3}; contour 4, 3×10^{-3}; contour 5, 4.5×10^{-3}; contour 6, 6.5×10^{-3}; and contour 7, 1×10^{-2}.

Type II Orbits

A second family of displaced orbits may now be generated by selecting $\omega = \sqrt{(\mu/\rho^3)}$. This family of orbits will then be synchronous with a body on a circular Keplerian orbit in the $z = 0$ plane with orbit radius ρ. It is found that the required pitch angle and thrust-induced acceleration are now given by

$$\tan\alpha = (\rho/z)\left[1 - [1 + (z/\rho)^2]^{\frac{3}{2}}\right] \tag{12a}$$

$$a = (\mu/r^2)\left[1 + [1 + (z/\rho)^2]^2\left[1 - 2[1 + (z/\rho)^2]^{-\frac{3}{2}}\right]\right]^{\frac{1}{2}} \tag{12b}$$

The required thrust-induced acceleration is again shown as a function of orbit radius and displacement in Fig. 2b.

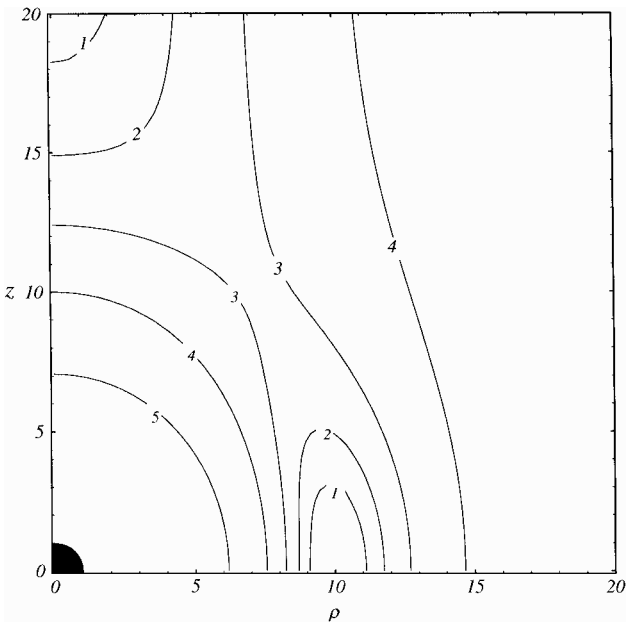

Fig. 2c Nondimensional acceleration contours for type III orbits: contour 1, 3×10^{-3}; contour 2, 4.5×10^{-3}; contour 3, 6.5×10^{-3}; contour 4, 1×10^{-2}; and contour 5, 2×10^{-2}.

Type III Orbits

A third family of orbits is obtained by fixing the orbit period to be constant throughout the ρ–z plane so that $\omega = \omega_0$. The required pitch angle and thrust-induced acceleration are given by

$$\tan\alpha = (\rho/z)\left[1 - (\omega_0/\omega_*)^2\right] \tag{13a}$$

$$a = \left[\rho^2\left(\omega_0^2 - \omega_*^2\right)^2 + z^2\omega_*^4\right]^{\frac{1}{2}} \tag{13b}$$

The required thrust-induced acceleration is shown in Fig. 2c for a value of ω_0 chosen such that the displaced orbits are synchronous with a Keplerian orbit with radius $\rho = 10$. As can be seen, there are two distinct branches of solutions corresponding to orbits in the $z = 0$ plane or orbits displaced above this plane.

IV. Orbit Stability

System Linearization

The equation of motion in the rotating frame of reference will now be linearized by adding a perturbation $\boldsymbol{\sigma}$ such that $\boldsymbol{r} \to \tilde{\boldsymbol{r}} + \boldsymbol{\sigma}$, where $\tilde{\boldsymbol{r}} = (\tilde{\rho}, \tilde{\phi}, \tilde{z})$ corresponds to the nominal displaced non-Keplerian orbit solution, with the thrust-induced acceleration fixed in both magnitude and direction. Then, Eq. (4) may be linearized to obtain a variational equation, viz.,

$$\ddot{\boldsymbol{\sigma}} + 2\boldsymbol{\omega} \times \dot{\boldsymbol{\sigma}} + \boldsymbol{\Lambda}\boldsymbol{\sigma} = 0, \qquad \boldsymbol{\Lambda} = \left[\frac{\partial \nabla U}{\partial \boldsymbol{r}}\right]_{\boldsymbol{r}=\tilde{\boldsymbol{r}}} \tag{14}$$

Defining the perturbations in $(\tilde{\rho}, \tilde{\phi}, \tilde{z})$ as (ξ, ψ, η) and extracting the azimuthal terms from Eq. (14), it is found that

$$\ddot{\psi} + (2\omega/\tilde{\rho})\dot{\xi} = 0 \tag{15}$$

which immediately integrates to

$$\dot{\psi} = -(2\omega/\tilde{\rho})\xi + C \tag{16}$$

where C is a constant of integration. This is a linearized form of Kepler's third law, relating the azimuthal drift $\dot{\psi}$ to the radial perturbation ξ. This relation may now be used to remove the first derivative terms from Eq. (14), which enables the variational equation to be written as

$$\begin{bmatrix}\ddot{\xi}\\ \ddot{\eta}\end{bmatrix} + \begin{bmatrix}\lambda_{11} & \lambda_{12}\\ \lambda_{21} & \lambda_{22}\end{bmatrix}\begin{bmatrix}\xi\\ \eta\end{bmatrix} = \begin{bmatrix}2\omega C\tilde{\rho}\\ 0\end{bmatrix} \tag{17}$$

Removing the tilde notation for clarity, the matrix elements may be written as

$$\lambda_{11} = 3\omega^2 + \omega_*^2[1 - 3(\rho/r)^2] \tag{18a}$$

$$\lambda_{12} = \lambda_{21} = -3\omega_*^2[\rho z/r^2] \tag{18b}$$

$$\lambda_{22} = \omega_*^2[1 - 3(z/r)^2] \tag{18c}$$

The constant term on the right-hand side of Eq. (17) may now be removed by a suitable coordinate transformation. Provided the determinant $\lambda_{11}\lambda_{22} - \lambda_{12}^2$ is nonzero, the transformation

$$\xi' = \xi - 2\omega C\rho\frac{\lambda_{22}}{\lambda_{11}\lambda_{22} - \lambda_{12}^2} \tag{19a}$$

$$\eta' = \eta + 2\omega C\rho\frac{\lambda_{12}}{\lambda_{11}\lambda_{22} - \lambda_{12}^2} \tag{19b}$$

allows Eq. (17) to be written in standard form as

$$\begin{bmatrix}\ddot{\xi}'\\ \ddot{\eta}'\end{bmatrix} + \begin{bmatrix}\lambda_{11} & \lambda_{12}\\ \lambda_{21} & \lambda_{22}\end{bmatrix}\begin{bmatrix}\xi'\\ \eta'\end{bmatrix} = \begin{bmatrix}0\\ 0\end{bmatrix} \tag{20}$$

The local stability characteristics of the three families of orbits can now be obtained in the usual manner through a solution to the variational equation of the form

$$\begin{bmatrix}\xi'\\ \eta'\end{bmatrix} = \begin{bmatrix}\xi_0\\ \eta_0\end{bmatrix}\exp(\gamma t) \tag{21}$$

The characteristic polynomial of the variational equation is then found to be

$$\gamma^4 + \gamma^2(\lambda_{11} + \lambda_{22}) + \left(\lambda_{11}\lambda_{22} - \lambda_{12}^2\right) = 0 \tag{22}$$

To guarantee nonpositive roots, and thus linear stability, it is required that the coefficients as well as the discriminant of the quadratic in γ^2 be positive. In the case of the discriminant, this can be shown to be true for all three orbit families. It should be noted that, because a linearization is performed, the analysis only provides necessary conditions for stability and sufficient conditions for instability. However, for class I orbits the conditions agree with the necessary and sufficient condition obtained in Ref. 6 using a fully nonlinear analysis in KS variables. For the remaining orbit families, numerical experiments suggest that these conditions for stability are, in fact, sufficient.

Type I Stability

Using the conditions for type I orbits it is found that

$$\lambda_{11} + \lambda_{22} = 2\omega_*^2 \tag{23a}$$

$$\lambda_{11}\lambda_{22} - \lambda_{12}\lambda_{21} = \omega_*^4[4 - 3(\rho/r)^2 - 12(z/r)^2] \tag{23b}$$

Because it is clear that Eq. (23a) is strictly positive, the necessary but not sufficient linear stability condition is satisfied if Eq. (23b) is strictly positive. This occurs when

$$\rho \succ 2\sqrt{2}z \tag{24}$$

As already noted, this condition has also been derived using a nonlinear analysis in KS variables,[6] which provides both necessary and sufficient conditions for stability. Therefore, stable and unstable subfamilies of type I orbits exist, partitioned by the cone defined by Eq. (24). Example stable and unstable type I orbits are shown in Fig. 3.

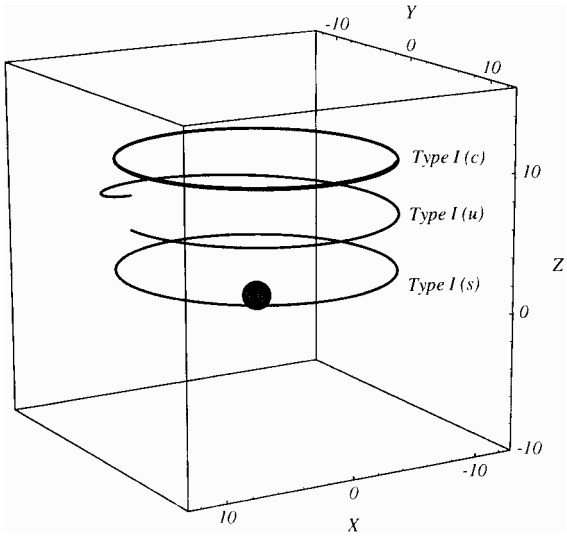

Fig. 3 Type I orbits: stable (s) ($\rho_0 = 10, z_0 = 2$), unstable (u) ($\rho_0 = 10, z_0 = 6$), and controlled (c) ($\rho_0 = 10, z_0 = 10, g_{1,3} = 0.3, g_{2,4} = 0.15$).

Type II Stability

Using the conditions for type II orbits, it is found that

$$\lambda_{11} + \lambda_{22} = -\omega_*^2[1 - 3(r/\rho)^2] \tag{25a}$$

$$\lambda_{11}\lambda_{22} - \lambda_{12}\lambda_{21} = -\omega_*^4[2 - 3(r/\rho)^3 + 9(rz^2/\rho^3)] \tag{25b}$$

Again, the first coefficient is strictly positive. In addition, the second coefficient is strictly positive if

$$\tfrac{2}{3}(\rho/r)^3 + 3(z/r)^2 - 1 \prec 0 \tag{26}$$

The boundary between linearly stable and unstable orbits can be obtained by substituting an equality in Eq. (26) and rewriting as

$$\tfrac{2}{3}[1 + (z/\rho)^2]^{-\frac{3}{2}} + 3(z/\rho)^2[1 + (z/\rho)^2]^{-1} - 1 = 0 \tag{27}$$

Clearly, Eq. (27) is a function z/ρ only. Therefore, the boundary between linearly stable and unstable orbits is of the form $\rho = \kappa z$, where κ is a constant. This constant may now be found from Eq. (27), viz.,

$$\tfrac{2}{3}(1 + \kappa^{-2})^{-\frac{3}{2}} + 3\kappa^{-2}(1 + \kappa^{-2})^{-1} - 1 = 0 \tag{28}$$

Further simplification is possible by making the substitution $\delta = (1 + \kappa^{-2})^{1/2}$ to clear the radical and to obtain

$$\delta^3 - \tfrac{3}{2}\delta + \tfrac{1}{3} = 0 \tag{29}$$

The solution to this cubic then yields $\kappa = 2.264$. The necessary but not sufficient condition for stability is, therefore,

$$\rho \succ 2.264z \tag{30}$$

which again defines a cone partitioning the linearly stable and unstable families of type II orbits.

Type III Stability

In general, this case requires a numerical solution of the stability criteria. However, for particular classes of orbits, a closed solution may be obtained, as detailed in Ref. 7.

V. Orbit Control

Now that orbit stability has been considered, linear control will be investigated as a means of stabilizing the unstable families of orbits. The variational equations may be cast in standard state-space form as

$$\dot{\boldsymbol{x}} = \boldsymbol{A}\boldsymbol{x} + \boldsymbol{B}\boldsymbol{u} \tag{31}$$

where the state vector $\boldsymbol{x} = [\xi, \eta, \dot{\xi}, \dot{\eta}]$ and

$$\boldsymbol{A} = \left[\begin{array}{c|c} \boldsymbol{0} & \boldsymbol{I} \\ \hline -\boldsymbol{\Lambda} & \boldsymbol{0} \end{array}\right], \qquad \boldsymbol{B} = \left[\begin{array}{c} \boldsymbol{0} \\ \hline \boldsymbol{K} \end{array}\right]$$

$$\boldsymbol{\Lambda} = \begin{bmatrix} \lambda_{11} & \lambda_{12} \\ \lambda_{21} & \lambda_{22} \end{bmatrix}, \qquad \boldsymbol{K} = \begin{bmatrix} K_1 \\ K_2 \end{bmatrix} \tag{32}$$

The control variable $\boldsymbol{u}$ to be considered will be trims in the pitch angle $\delta\alpha$, with a fixed thrust-induced acceleration, or variations in the acceleration δa, with a fixed pitch angle. With pitch control it is found that

$$\boldsymbol{K} = [a\cos\alpha, -a\sin\alpha]^T \tag{33a}$$

and with acceleration control it is found that

$$\boldsymbol{K} = [a\sin\alpha, a\cos\alpha]^T \tag{33b}$$

The controllability of these two modes of control in the ρ–z plane may be determined from the matrix $\boldsymbol{C} = [\boldsymbol{B}, \boldsymbol{AB}, \boldsymbol{A}^2\boldsymbol{B}, \boldsymbol{A}^3\boldsymbol{B}]$. Substituting for the appropriate matrices from Eq. (32) it is found that

$$\boldsymbol{C} = \begin{bmatrix} 0 & K_1 & 0 & -\lambda_{11}K_1 - \lambda_{12}K_2 \\ 0 & K_2 & 0 & -\lambda_{21}K_1 - \lambda_{22}K_2 \\ K_1 & 0 & -\lambda_{11}K_1 - \lambda_{12}K_2 & 0 \\ K_2 & 0 & -\lambda_{21}K_1 - \lambda_{22}K_2 & 0 \end{bmatrix} \tag{34}$$

For controllability it is necessary that the matrix $\boldsymbol{C}$ has full rank. Because $\boldsymbol{C}$ is square, this is equivalent to the matrix being nonsingular. It is found that the determinant of the matrix is given by

$$\|\boldsymbol{C}\| = K_1(\lambda_{21}K_1 + \lambda_{22}K_2) - K_2(\lambda_{11}K_1 + \lambda_{12}K_2) \tag{35}$$

The condition for noncontrollability and, hence $\|\boldsymbol{C}\| = 0$, is found to be

$$\sin\alpha\cos\alpha = \frac{2\rho z}{(\omega/\omega_*)^2(z^2 + \rho^2) + (z^2 - \rho^2)} \tag{36}$$

for pitch control and

$$\sin\alpha\cos\alpha = -\frac{2\rho z}{(\omega/\omega_*)^2(z^2 + \rho^2) + (z^2 - \rho^2)} \tag{37}$$

for acceleration control. For type I orbits the condition for noncontrollability for the two control modes then reduces to

$$\sin\alpha\cos\alpha = \pm[\rho/z] \tag{38}$$

Therefore, type I orbits are always controllable provided that $\rho \neq 0$. It is found that the other families of orbits are also controllable in general.

To illustrate the use of linear control, stabilization of an unstable type I orbit will be considered. Full state feedback will be used along with pitch control, viz.,

$$\delta\alpha = g_1\xi + g_2\dot{\xi} + g_3\eta + g_4\dot{\eta} \tag{39}$$

The selection of the gains ($g_i, i = 1$–4) is made using standard methods. An example of a controlled orbit is shown in Fig. 3 using this state feedback law. It is clear that in practice a state estimator would be required if all state variables are to be used in the feedback control law. Such state sensing and estimation is beyond the scope of the current discussion.

VI. Spiral Orbits

It will now be shown that displaced non-Keplerian orbits may be modified into spiral orbits using a transverse component of thrust a_ϕ. For ease of illustration, the equations of motion for a displaced type I orbit will be cast in cylindrical polar coordinates in the inertial frame of reference I, viz.,

$$\ddot{\rho} - \rho\dot{\phi}^2 = -(\mu/r^2)[\rho/r] \tag{40a}$$

$$\rho\ddot{\phi} + 2\dot{\rho}\dot{\phi} = a_\phi \tag{40b}$$

$$\ddot{z} = -(\mu/r^2)[z/r] + a_z \tag{40c}$$

where the acceleration components a_z and a_ϕ are constant. In particular, the vertical acceleration component a_z corresponds to that required for a type I orbit. Then, assuming that the out-of-plane displacement is small relative to the orbit radius, Eqs. (40) may be written as

$$\ddot{\rho} - \rho\tilde{\omega}^2 = -(\mu/\rho^2) \tag{41a}$$

$$\rho\dot{\tilde{\omega}} + 2\dot{\rho}\tilde{\omega} = a_\phi \tag{41b}$$

$$\ddot{z} = -(\mu/\rho^2)[z/\rho] + a_z \tag{41c}$$

where $\tilde{\omega} = \dot{\phi}$ is the local orbital angular velocity. If, in addition, it is now assumed that the spiral is quasicircular such that $\ddot{\rho} \approx 0$ and $\ddot{z} \approx 0$, Eq. (41a) then yields

$$\tilde{\omega} = \sqrt{\mu/\rho^3} \tag{42}$$

Therefore, substituting this result in Eq. (41b) yields

$$\dot{\rho} = (2a_\phi/\sqrt{\mu})\rho^{\frac{3}{2}} \tag{43}$$

Then, noting from Eq. (11b) that $a_z = \mu z_0/\rho_0^3$, where ρ_0 and z_0 are the initial orbit radius and displacement, Eq. (41c) yields

$$z = z_0[\rho/\rho_0]^3 \tag{44}$$

Last, Eqs. (43) and (44) may be integrated to provide the orbit radius and out-of-plane displacement as the spacecraft spirals, viz.,

$$\rho = \rho_0\left[1 - \sqrt{(\rho_0/\mu)}a_\phi t\right]^{-2} \tag{45a}$$

$$z = z_0\left[1 - \sqrt{(\rho_0/\mu)}a_\phi t\right]^{-6} \tag{45b}$$

An example outward spiral trajectory obtained by numerical integration is shown in Fig. 4. It can be seen that the out-of-plane displacement increases as the spacecraft spirals outward, due to the decreasing vertical component of gravity, as is evident from Eq. (44). It is found that Eqs. (45) provide an accurate representation of such displaced spiral trajectories.

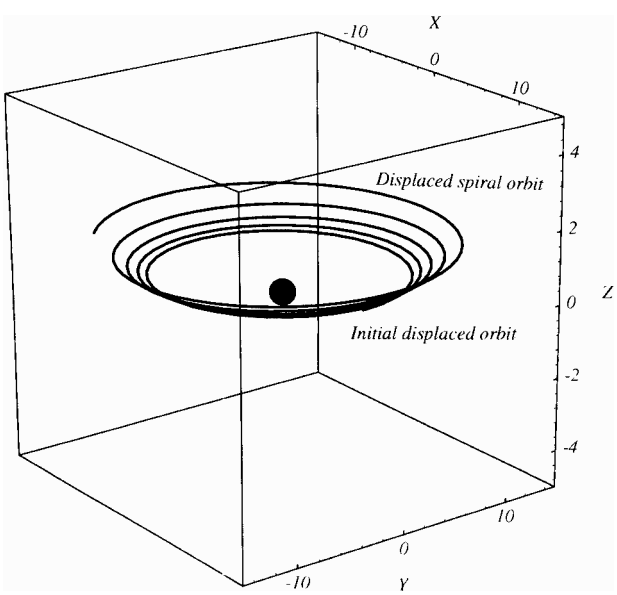

Fig. 4 Displaced spiral orbit with $\rho_0 = 10, z_0 = 0.5$, and $a_\phi = 10^{-2}\, a_z$.

VII. Impulse Control

The displaced orbits investigated in Sec. III may also be generated using impulse control. In this case the out-of-plane displacement is achieved by repeatedly reversing the vertical component of the spacecraft velocity in a periodic manner. To compare the continuous thrust and impulse control orbits, linearized equations of motion will now be considered for small displacements, as shown in Fig. 5. The linearized Hill equations[8] represent the dynamics of the spacecraft in the vicinity of a fixed point P on a circular reference orbit, viz.,

$$\ddot{x} - 2\omega\dot{y} - 3\omega^2 x = a_x \tag{46a}$$

$$\ddot{y} + 2\omega\dot{x} = a_y \tag{46b}$$

$$\ddot{z} + \omega^2 z = a_z \tag{46c}$$

where $\omega = \sqrt{(\mu/R^3)}$ is now the orbital angular velocity of the fixed point P on the circular reference orbit and (x, y, z) corresponds to a local frame attached to this point. If the spacecraft station keeps out-of-plane relative to this point, the resulting orbit will then correspond to a type III displaced orbit. If there are no control accelerations, the Hill equations have a solution of the form

$$x(t) = [\dot{x}_0/\omega]\sin(\omega t) - [3x_0 + (2\dot{y}_0/\omega)]\cos(\omega t) + [(2\dot{y}_0/\omega) + 4x_0] \tag{47a}$$

$$y(t) = [(4\dot{y}_0/\omega) + 6x_0]\sin(\omega t) + [2\dot{x}_0/\omega]\cos(\omega t) - [3\dot{y}_0 + 6\omega x_0]t + [y_0 - (2\dot{x}_0/\omega)] \tag{47b}$$

$$z(t) = z_0\cos(\omega t) + (\dot{z}_0/\omega)\sin(\omega t) \tag{47c}$$

which will be used later in this section.

For continuous thrust, the required acceleration components for displaced solutions may be obtained from Eqs. (46) as

$$a_x = -3\omega^2 x \tag{48a}$$

$$a_y = 0 \tag{48b}$$

$$a_z = \omega^2 z \tag{48c}$$

A similar displaced orbit may also be obtained by impulse control, as will now be demonstrated. To maintain an out-of-plane displacement, repeated vertical impulses are required such that $z(T) = z_0$, where T is the period between impulses. Then, using Eq. (47c) the required out-of-plane velocity at the start of the cycle is given by

$$\dot{z}_0 = \omega z_0 \tan[\omega T/2] \tag{49}$$

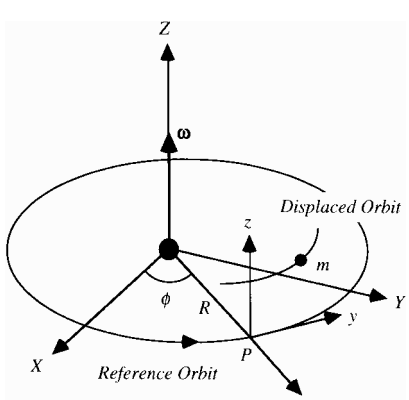

Fig. 5 Orbit reference frame for impulse control.

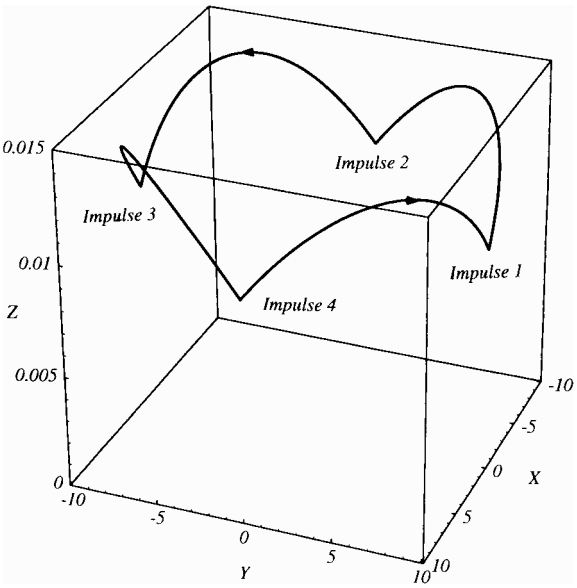

Fig. 6 Displaced orbit with impulse control every quarter orbit: $R = 10$, $x_0 = 0.01$, and $z_0 = 0.01$.

Because $\dot{z}(T) = -\dot{z}(0)$, the effective out-of-plane acceleration $\bar{a}_z$ provided by the repeated impulses is then $2\dot{z}(0)/T$ so that

$$\bar{a}_z = (2\omega z_0/T)\tan[\omega T/2] \tag{50}$$

If the time between impulses is small Eq. (50) can be expanded to yield

$$\bar{a}_z = \omega^2 z_0 + \tfrac{1}{12}\omega^4 z_0 T^2 + \cdots \tag{51}$$

Comparing Eqs. (51) and (48c) it can be seen that to first order the required accelerations are equal, with higher-order corrections representing the increased load required for impulse control.

For a radial displacement, the condition $y(0) = 0$ will be used along with the requirements $y(T) = 0$ and $x(T) = x_0$. Again using Eqs. (47a) and (47b), it is found that the required initial velocity components are given by

$$\dot{x}(0) = \frac{3\omega^2 T x_0 \sin(\omega T/2)}{3\omega T\cos(\omega T/2) - 8\sin(\omega T/2)} \tag{52a}$$

$$\dot{y}(0) = -6\omega x_0 \frac{\omega T\cos(\omega T/2) - 2\sin(\omega T/2)}{3\omega T\cos(\omega T/2) - 8\sin(\omega T/2)} \tag{52b}$$

However, it is found that $\dot{y}(T) = \dot{y}(0)$ and $\dot{x}(T) = -\dot{x}(0)$ so that only repeated radial impulses are required. The effective radial acceleration $\bar{a}_x$ provided by the repeated impulses is then $2\dot{x}(0)/T$. Expanding Eq. (52a) for small impulse periods T, it is found that

$$\bar{a}_x = -3\omega^2 x_0 + \tfrac{3}{4}\omega^4 x_0 T^2 + \cdots \tag{53}$$

Again, comparing Eqs. (53) and (48a) it can be seen that to first order the required accelerations are equal. An example orbit is shown in Fig. 6 viewed from an inertial frame of reference. Impulse control is used every quarter orbit to provide a small out-of-plane displacement and a small radial displacement relative to the reference orbit at $R = 10$.

VIII. Patched Orbits

In this section it will be demonstrated that displaced non-Keplerian orbits may be patched together, providing additional families of orbits, as shown in Fig. 7. First, displaced orbits will be patched to Keplerian orbits by nulling the spacecraft thrust. Then, the conditions required to transfer between displaced non-Keplerian orbits will be considered.

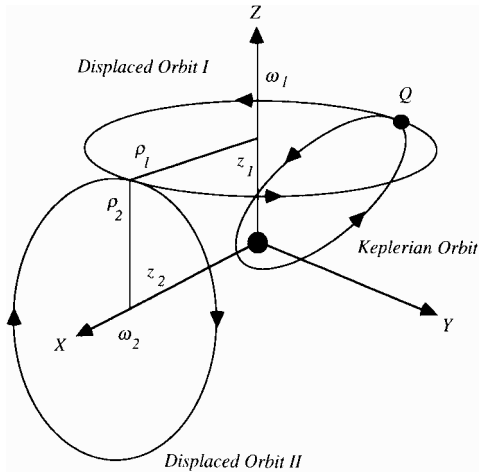

Fig. 7 Schematic of patched orbits.

Patch to Keplerian Orbit

For a displaced circular non-Keplerian orbit, the spacecraft thrust vector is always normal to the spacecraft velocity vector so that the total energy E is constant, viz.,

$$E = \tfrac{1}{2}\omega^2\rho^2 - \frac{\mu}{\sqrt{\rho^2 + z^2}} \tag{54}$$

Therefore, because $E = -\mu/2a$, the semimajor axis of the Keplerian orbit obtained by nulling the spacecraft acceleration is given by

$$a = \left[\frac{2}{\sqrt{\rho^2 + z^2}} - \frac{\omega^2\rho^2}{\mu}\right]^{-1} \tag{55}$$

Similarly, noting that the patch point Q corresponds to the apocenter of the Keplerian orbit, viz.,

$$a(1 + e) = \sqrt{\rho^2 + z^2} \tag{56}$$

the eccentricity may be also obtained as

$$e = 1 - (\omega^2\rho^2/\mu)\sqrt{\rho^2 + z^2} \tag{57}$$

Therefore, for a given displaced non-Keplerian orbit, the size and shape of the Keplerian orbit obtained by nulling the spacecraft thrust are obtained. A schematic transfer is shown in Fig. 7.

Patch to Non-Keplerian Orbit

Now that patching to Keplerian orbits has been considered, the requirements for patching to other circular displaced non-Keplerian orbits will be investigated. Two orbits that meet tangentially will be considered, as shown in Fig. 7. For velocity continuity between the orbits the following condition is required, viz.,

$$\rho_1\omega_1 = \rho_2\omega_2 \tag{58}$$

Similarly from Eq. (10b), and noting that $\rho_1^2 + z_1^2 = \rho_2^2 + z_2^2$, the condition for continuity of thrust-induced acceleration is given by

$$\rho_1^2\omega_1^2\left(\omega_1^2 - 2\omega_*^2\right) = \rho_2^2\omega_2^2\left(\omega_2^2 - 2\omega_*^2\right) \tag{59}$$

However, using Eq. (58), it can be seen from Eq. (59) that the condition $\omega_1 = \omega_2$, and so $\rho_1 = \rho_2$ is required. Therefore, the two orbits must be identical, but perpendicular to each other. By relaxing the requirement for continuity of thrust-induced acceleration, it is found that more complex families of orbits can be generated.

Table 1 Requirements for a type II orbit displaced above Saturn's A ring

Altitude, km	5	10	20	50
a, mms^{-2}	0.01	0.02	0.41	1.03
Δv,[a] ms^{-1}	4.53	9.06	18.12	45.30
Δv,[b] ms^{-1}	4.69	9.37	18.74	46.86

[a]Accumulated Δv per orbit for low-thrust propulsion.
[b]Accumulated Δv per orbit for impulse control (10 impulses per orbit).

IX. In Situ Observations of Saturn's Rings

Previous studies[2] have identified displaced orbits as a means of studying Saturn's rings in situ. Clearly spacecraft in the ring plane are at risk from impacts from ring particles, whereas spacecraft displaced above the ring plane using low-thrust propulsion may safely provide high-resolution images of the ring system below. Type II provides a family of orbits that are ideally suited to such applications. These orbits are synchronous with a body at the same radius orbiting in the $z = 0$ plane. Therefore, using type II orbits, the spacecraft may be displaced above the ring system but will orbit synchronously with ring features directly below. In addition, such orbits will be stable for small displacements above the ring system. Similarly, type III orbits may be used to provide motion synchronous with a particular ring feature.

For example, a type II orbit displaced 20 km above the inner edge of the A ring at 2.025 planetary radii requires an acceleration of only 4.1×10^{-4} ms^{-2} (Δv of 18.1 ms^{-1} per orbit). The orbit period is 12.1 h, synchronous with the ring features directly below. For impulse control, using 10 impulses per orbit, the required Δv is 18.7 ms^{-1} per orbit. The requirements for other A-ring orbits are shown in Table. 1. It may be noted that the thickness of the A ring is estimated to be of order 1 km. (Ref. 9). By nulling the thrust-induced acceleration the spacecraft may transfer to an inclined elliptical orbit that takes it through and below the ring plane. After one orbit the spacecraft may then transfer back to the original displaced non-Keplerian orbit, albeit at a different azimuthal location. In addition, by rotating the thrust vector to generate a small transverse acceleration, the spacecraft may spiral inward through the ring system. For example, when the spacecraft has spiralled to 1.5 planetary radii, the initial 20 km out-of-plane displacement will fall to 8.1 km due to the increased vertical component of gravity.

X. Conclusions

It has been shown that large families of displaced non-Keplerian orbits exist. These families have both linearly stable and unstable subfamilies. However, it has been shown that the unstable subfamilies are controllable and so may be stabilized through the use of linear state feedback control. As an alternative to continuous thrust, impulse control has also been investigated as a means of generating displaced orbits. The addition of a small transverse component of thrust has been shown to yield displaced spiral orbits. In addition, it has been shown that displaced orbits may be patched to Keplerian orbits and to other displaced non-Keplerian orbits generating additional new families.

References

[1]Austin, R. E., Dod, R. E., and Terwilliger, C. H., "The Ubiquitous Solar Electric Propulsion Stage," *Acta Astronautica*, Vol. 4, 1977, pp. 671–694.

[2]Nock, K. T., "Rendezvous with Saturn's Rings," *Anneux des Planetes*, IAU Colloquium No. 75, Cepadues, Toulouse, France, 1984, p. 743.

[3]McInnes, C. R., "Solar Sail Halo Trajectories: Dynamics and Applications," 42nd International Astronautical Federation Congress, IAF Paper 91-334, Montreal, PQ, Canada, Oct. 1991.

[4]McInnes, C. R., and Simmons, J. F. L., "Solar Sail Halo Orbits I: Heliocentric Case," *Journal of Spacecraft and Rockets*, Vol. 29, No. 4, 1992, pp. 466–471.

[5]McInnes, C. R., and Simmons, J. F. L., "Solar Sail Halo Orbits II: Geocentric Case," *Journal of Spacecraft and Rockets*, Vol. 29, No. 4, 1992, pp. 472–479.

[6]Dankowicz, H., "Some Special Orbits in the Two-Body Problem with Radiation Pressure," *Celestial Mechanics and Dynamical Astronomy*, Vol. 58, No. 4, 1994, pp. 353–370.

[7]McInnes, C. R., "Existence and Stability of Families of Displaced Two-Body Orbits," *Celestial Mechanics and Dynamical Astronomy*, Vol. 67, No. 2, 1997, pp. 167–180.

[8]Sidi, M. J., *Spacecraft Dynamics and Control*, Cambridge Univ. Press, Cambridge, England, UK, 1997, pp. 57–59.

[9]Cuzzi, J. N., Lissauer, J. J., Esposito, L. W., Holberg, J. B., Marouf, E. A., Tyler, G. L., and Boischot, A., "Saturn's Rings: Properties and Processes," *Planetary Rings*, edited by R. Greenberg and A. Brahic, Univ. of Arizona Press, Tucson, AZ, 1984, pp. 73–199.